Competitive oxygen-18 kinetic isotope effects expose O–O bond formation in water oxidation catalysis by monomeric and dimeric ruthenium complexes†

Alfredo M. Angeles-Boza,‡[a] Mehmed Z. Ertem,§*[b] Rupam Sarma,[a]
Christian H. Ibañez,[a] Somnath Maji,[c] Antoni Llobet,*[c] Christopher J. Cramer[b]
and Justine P. Roth*[a]

Competitive oxygen kinetic isotope effects (^{18}O KIEs) on water oxidation initiated by ruthenium oxo (Ru=O) complexes are examined here as a means to formulate mechanisms of O–O bond formation, which is a critical step in the production of "solar hydrogen". The kinetics of three structurally related catalysts are investigated to complement the measurement and computation of [18]O KIEs, derived from the analysis of O_2 relative to natural abundance H_2O under single and multi-turnover conditions. The findings reported here support and extend mechanistic proposals from [18]O tracer studies conducted exclusively under non-catalytic conditions. It is shown how density functional theory calculations, when performed in tandem with experiments, can constrain mechanisms of catalytic water oxidation and help discriminate between them.

Introduction

Light-driven water oxidation provides the protons and electrons that reduce carbon dioxide to glucose during oxygenic photosynthesis.[1] Formation of the O–O bond in molecular oxygen has been proposed to represent the highest energy barrier in the reaction (eqn (1)), making catalysis of this step an important objective.[2–4] Competitive oxygen-18 kinetic isotope effects (^{18}O KIEs) are applied here to probe mechanisms of water oxidation catalysis and interpreted using density functional theory (DFT) for the first time.

$$2H_2O + sunlight \xrightarrow[\text{catalyst}]{} O_2 + 4H^+ + 4e^- \qquad (1)$$
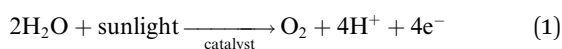
Ideally, the oxides of earth abundant transition metals could be used for photochemical conversion of water to "solar

[a]Department of Chemistry, Johns Hopkins University, 3400 North Charles Street, Baltimore, MD 21218, USA. E-mail: jproth@jhu.edu

[b]Department of Chemistry and Supercomputing Center, University of Minnesota, 207 Pleasant St. SE, Minneapolis, MN 55455, USA

[c]Institute of Chemical Research of Catalonia (ICIQ), Av. Països Catalans, 16, 43007 Tarragona, Spain

† Electronic supplementary information (ESI) available: Full experimental characterization and computational details. See DOI: 10.1039/c3sc51919h

‡ Present addresses: University of Connecticut, Department of Chemistry, 55 North Eagleville Road, Storrs, CT 06269, USA.

§ Present addresses: Yale University, Department of Chemistry, P.O. Box 208107, New Haven, CT 08107-06520 and The Chemistry Department, Brookhaven National Laboraory, Bldg. 555A, Upton, NY – 11973, USA.

hydrogen", producing the cleanest and most sustainable source of energy for "powering the planet".[5] Significant improvements in catalyst performance are needed, however, to make artificial photosynthesis a viable alternative to burning fossil fuels. Progress in this area would be revolutionary, reducing toxic gas emissions[6] and the devastation of natural environments[7] while bolstering the global economy.[8]

A major objective in the basic energy sciences is to improve homogenous water oxidation catalysis. To this end, mechanistic understanding of the O–H bond breaking and O–O bond making steps in eqn (1) is needed.[1,9,10] In this study, it is shown how such insights can be obtained through competitive isotopic measurements and prediction of the resulting [18]O KIEs using DFT methods, together with Transition State Theory.[11,12]

Oxygen isotope fractionation (from natural abundance levels) was originally developed by geologists and plant biologists as a technique for monitoring photosynthetic water oxidation and carbon dioxide fixation based on ^{18}O/^{16}O ratios.[13–15] The same basic methodology has since been applied to probe simple chemical transformations of O_2, superoxide (O_2^-) and hydrogen peroxide (H_2O_2).[11] DFT calculations have been indispensible to these efforts allowing for the modeling of transition states. In this study, competitive [18]O KIEs are determined from the O_2 produced upon water oxidation initiated by the ruthenium complexes in Fig. 1.[16–19]

In contrast to isotope tracer studies, conducted with ^{18}O-labeled ruthenium complexes under stoichiometric conditions to prevent H_2O exchange on the timescale of experiments,[16a,17a,d,18c] competitive [18]O KIE measurements can be
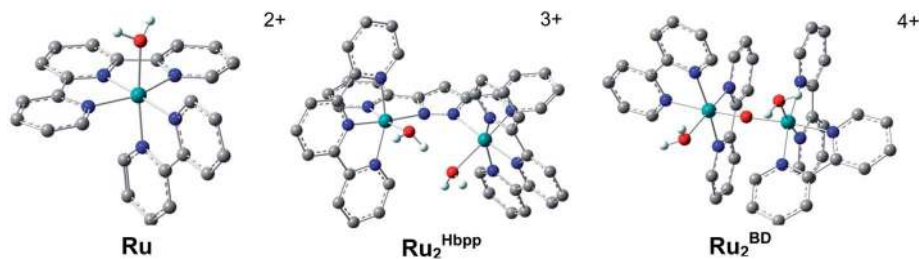
Fig. 1 The ruthenium perchlorate complexes[19,20] used as initiators of water oxidation catalysis are abbreviated as follows: $[Ru^{II}(bpy)(tpy)(OH_2)](ClO_4)_2$ (**Ru**, bpy = 2,2′ bipyridine, tpy = 2,2′:6′,2″-terpyridine), $[Ru^{II,II}(tpy)_2(OH_2)_2(\mu\text{-bpp})](ClO_4)_2$ (**Ru$_2$^{Hbpp}**, Hbpp = bis(2-pyridyl)-3,5-pyrazolate) and cis,cis-$[Ru^{III}(bpy)_2(OH_2)(\mu\text{-O})]_2(ClO_4)_4$ (**Ru$_2$^{BD}**).

used to probe single turnover as well as multi-turnover catalytic reactions. Isotopic fractionation analysis of H_2O requires a specialized vacuum apparatus[13a] to hermetically manipulate samples, quantitatively isolate O_2 and purify this product from other condensable gases (none was found to form in control experiments conducted at atmospheric pressure). The O_2 is completely combusted to CO_2 and its pressure determined before condensation into a dried glass tube, which is then flame-sealed. Sample analysis employs dual-inlet isotope ratio mass spectrometry (IRMS).[21] IRMS allows $^{18}O/^{16}O$ content to be determined with errors of ± 0.0002. Experimental manipulations can inflate the error by an order of magnitude, which is still more than an order of magnitude less than the ^{18}O KIEs measured in this study.

Results

Steady-state kinetics

Steady-state rate constants were determined by analyzing initial rates of O_2 production by water oxidation catalysis using a Clark-type electrode at $22.0 \pm 0.2\ °C$, as previously described.[21]

Ceric ammonium nitrate, $(NH_4)_2Ce^{IV}(NO_3)_6$ or CAN, served as the sacrificial oxidant in 0.1 M perchloric acid and triflic acid solutions prepared from H_2O or D_2O. Ionic strength (μ) was maintained at 1.0 M by addition of lithium perchlorate or sodium triflate. Reactions were initiated by introducing 1–10 µL aliquots of **Ru**, **Ru$_2$^{BD}** or **Ru$_2$^{Hbpp}** stock solutions into stirring, air-saturated 1.0–1.5 mL solutions, containing CAN. Initial rates of O_2 production, measured after allowing ~5 seconds for mixing, were found to vary in direct proportion to the concentration of **Ru**, **Ru$_2$^{BD}** and **Ru$_2$^{Hbpp}**.[19]

Prior kinetic investigations focused on rates at sub-saturating concentrations of CAN without control over ionic strength.[16–18,21] Here a wide range of CAN concentrations were examined to reveal hyperbolic and sigmoidal trends leading to kinetic saturation during catalysis (Fig. 2). The normal hyperbolic behaviors observed for **Ru$_2$^{BD}** and **Ru$_2$^{Hbpp}** are consistent with millimolar pre-equilibrium constants that describe interactions with CAN prior to an irreversible CAN-independent step. The sigmoid dependence observed with **Ru** is more complicated and suggests catalyst activation as the CAN concentration increases.
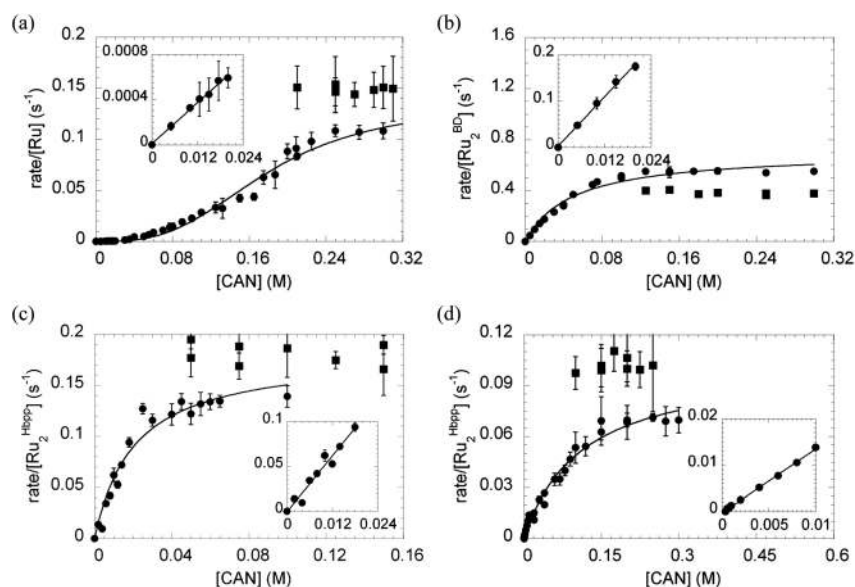

Fig. 2 Catalytic rate constant for H_2O (circles) and D_2O (squares) oxidation at variable CAN concentrations for reactions initiated by **Ru** (a), **Ru$_2$^{BD}** (b) or **Ru$_2$^{Hbpp}** (c) in 0.1 M perchloric acid and **Ru$_2$^{Hbpp}** in 0.1 M triflic acid (d).

Initial rate data in Fig. 2 were collected under conditions related to those used to measure ^{18}O KIEs and fitted to the expression: rate/[catalytic initiator] $= k_{cat}[CAN]^n/\{K_{CAN}^n + [CAN]^n\}$ to determine the parameters compiled in Table 1. The coefficient $n = 1$ for $\mathbf{Ru_2^{Hbpp}}$ and $\mathbf{Ru_2^{BD}}$, whereas $n = 3$ for $\mathbf{Ru}$. The latter implies that three equivalents of $(NH_4)_2Ce^{IV}(NO_3)_6$ or some derivative[22] reacts with $\mathbf{Ru}$ to cause rate enhancement. The hyperbolic fit for $\mathbf{Ru_2^{Hbpp}}$ and $\mathbf{Ru_2^{BD}}$ gives the second order rate constant k_{cat}/K_{CAN}, which can also be determined from linear regression analyses at sufficiently low CAN concentrations (Fig. 2 insets). The latter was used to determine k_{cat}/K_{CAN} for $\mathbf{Ru}$ (Table 1).

The k_{cat}/K_{CAN} and k_{cat}, are CAN-dependent and CAN-independent bimolecular and unimolecular rate constants. The former is defined beginning with CAN association leading up to and including the first irreversible step. The latter is defined as the catalyst turnover frequency at kinetically saturating CAN concentration. O–O bond formation may be a common step that limits both k_{cat}/K_{CAN} and k_{cat}. In this case, K_{CAN}, the ratio of the two parameters, reflects all equilibria preceding the turnover-controlling step. Alternatively, K_{CAN} represents a complex ratio of kinetic constants in units of concentration (M).

For the dimeric catalysts that exhibit hyperbolic kinetics, the trends in K_{CAN} could have implications. In perchloric acid, K_{CAN} is smaller for $\mathbf{Ru_2^{BD}}$ than $\mathbf{Ru_2^{Hbpp}}$ implying a more favorable pre-equilibrium, where oxidation by CAN is more facile for $\mathbf{Ru_2^{BD}}$. In addition, K_{CAN} for $\mathbf{Ru_2^{Hbpp}}$ is less favorable in triflic acid than perchloric acid suggesting a destabilizing effect of the counter-anion on the ground state thermodynamics.

Solvent deuterium kinetic isotope effects on k_{cat}, indicative of reactions with water, were determined in H_2O or D_2O. A slightly inverse to negligible effect of 0.92 ± 0.08 is indicated for $\mathbf{Ru}$. This result is close to unity, just as reported in perchloric acid at lower albeit uncontrolled ionic strength; the same study reported an inverse solvent isotope effect of 0.43 in nitric acid.[16c] $\mathbf{Ru_2^{BD}}$ exhibited a normal solvent deuterium isotope effect of 1.85 ± 0.16 under the conditions described. In contrast, no solvent isotope effect was discernible for $\mathbf{Ru_2^{Hbpp}}$ in perchloric acid or triflic acid.

Small normal to small inverse solvent deuterium isotope effects could arise for a number of reasons including but not limited to secondary isotope effects and competing processes. In the first case, an inverse secondary effect could arise from hydrogen-bonding of the solvent during its oxidation. In the second case, an inverse pre-equilibrium solvent isotope effect on the pK_a could offset a normal primary kinetic effect upon O–

H(D) bond cleavage. The latter scenario could occur if pre-equilibrium protonation of a metal oxo were required for O–O bond formation, as recently demonstrated in ferrate-mediated water oxidation.[11] The normal sign and magnitude of the solvent deuterium isotope effect on k_{cat} is entirely consistent with H/D transfer concomitant with O–O bond formation in the first irreversible step of catalyst turnover.[23]

Competitive oxygen-18 kinetic isotope effects

^{18}O KIEs on water oxidation were measured using an established competitive methodology.[11,21] Solutions were saturated with He prior to initiating reactions by addition of the dissolved oxidant (CAN in 0.1 M $HClO_4$ at pH 1.0) to the catalyst or the dissolution of both solids at the same time. $[Ru^{III}(bpy)_3]^{3+}$ was photo-generated in 0.050 M potassium phosphate buffer (KP_i) at pH 7.2. This procedure employs exhaustive photolysis of solutions containing $[Ru^{II}(bpy)_3](Cl)_2$ and potassium persulfate ($K_2S_2O_8$) as previously described.[21,24] No significant background production of O_2 was detectable.

The $^{18}O/^{16}O$ ratios were determined by IRMS analysis of CO_2 samples prepared from O_2 (by combustion) and from H_2O (by exchange with carbonate), following published protocols.[25] All results were referenced to Vienna Standard Mean Ocean Water (VSMOW).[26,27] At very low reactant conversions, as is the case for water oxidation, the ^{18}O KIE approximately equals the ratio of ratios given by eqn (2).[28] Terms include R_p for the $^{18}O/^{16}O$ of the O_2 product and R_0 for the $^{18}O/^{16}O$ of the source H_2O. Numerous determinations of the latter gave $R_0 = 0.9940 \pm 0.0008$ $vs.$ VSMOW.[11,21,28] Thus, the competitive ^{18}O KIEs were derived from analysis of R_0, representing the average of all samples of H_2O, divided by the R_p of the O_2 produced in single and multiturnover reactions.

$$^{18}O \text{ KIE} \cong \frac{R_0}{R_p} \qquad (2)$$

Eqn (2) is actually a special case of eqn (3),[31] which describes isotopic fractionation of the reactant at varying conversions, (f). In this study 1-f is equivalent to the H_2O remaining, calculated from the pressure of O_2. The change in $^{18}O/^{16}O$ within the reactant, R_f, is calculable from the relationship: $R_0 = R_f(1 - f) + R_p(f)$ while accounting for the reaction stoichiometry of eqn (1). The analysis performed according to eqn (3) gives an ^{18}O KIE in good agreement with eqn (2), although the errors are reduced by an order of magnitude.[11] To be conservative, the results in this study were derived from eqn (2) and quoted with errors of one

Table 1 Limiting kinetic constants and the free energy barrier for water oxidation in acidic media[a]

Initiator	k_{cat}/K_{CAN} ($M^{-1} s^{-1}$)	k_{cat} (s^{-1})	$^{D_2O}k_{cat}$[b] (s^{-1})	$\Delta G^{\ddagger}_{unimolecular}$ (kcal mol^{-1})
Ru	0.0301 ± 0.0024[c]	0.136 ± 0.011	0.148 ± 0.008	18.7 ± 1.4
Ru_2^{BD}	8.87 ± 0.64	0.704 ± 0.054	0.380 ± 0.032	17.8 ± 1.4
Ru_2^{Hbpp}	5.20 ± 0.84	0.181 ± 0.024	0.184 ± 0.020	18.6 ± 2.5
Ru_2^{Hbpp}[d]	1.38 ± 0.44	0.103 ± 0.011	0.102 ± 0.004	18.9 ± 2.0

[a] At 22.0 ± 0.2 °C, pH or pD 1.0 and $\mu = 1.0$ M. [b] Measured in D_2O. [c] Extracted from the linear phase shown in the insets of Fig. 2. [d] Data were collected in 0.1 M triflic acid at $\mu = 1.0$ M.

standard deviation about the mean of >15 independent experiments.

$$^{18}\text{O KIE} = \left[1 + \frac{\ln(R_f/R_0)}{\ln(1-f)}\right]^{-1} \quad (3)$$

Importantly, the same ^{18}O KIEs were determined at different turnover numbers as well as variable CAN concentrations under acidic conditions (Fig. 3). These data provide compelling evidence of a common O–O bond formation step (*vide infra*). Normal ^{18}O KIEs are observed, varying from 1.0172 ± 0.0020 for **Ru₂**^{BD} to 1.0313 ± 0.0027 for **Ru** to 1.0346 ± 0.0021 for **Ru₂**^{Hbpp}. Experiments were also conducted under photocatalytic conditions, in the presence of $[\text{Ru}^{III}(\text{bpy})_3]^{3+}$ in 0.05 M KP$_i$ buffer at neutral pH. In the latter experiments, the ^{18}O KIEs were 1.0051 ± 0.0035 for **Ru₂**^{BD} and 1.0143 ± 0.0028 for **Ru** suggesting a variation in a particular transition state structure or a change in the first irreversible step. Comparisons to **Ru₂**^{Hbpp} were not possible due to the absence of photocatalytic O₂ production under the conditions used for the other complexes.[21]

Computational methods

All geometries were fully-optimized at two levels of DFT.[29] One approach employed the previously validated *m*PW functional,[30] the LANL2DZ[31] pseudopotential basis set for Ru, 6-311G(d) basis set for O and N, and 6-31G basis set for C and H.[32] The second approach employed the M06-L functional,[33] along with the Stuttgart [8s7p6d2f|6s5p3d2f] ECP28MWB contracted pseudo-potential basis set[34] for Ru and 6-31G(d) basis[35] for all other atoms. Stationary points were verified by the analytic computation of vibrational frequencies and intrinsic reaction coordinate (IRC) calculations.[36]

Bulk solvation effects on the free energy barriers to O–O bond formation were included using the SMD aqueous continuum solvation model,[37] which in some cases involved applying single point corrections.[19] Several structures in proposed water oxidation mechanisms feature electronic structures that are not well-described by a single determinant so that the standard Kohn–Sham DFT is not directly applicable for

the accurate prediction of properties such as spin.[38] In such instances, the Yamaguchi broken-spin-symmetry (BS) procedure[39] was used to compute the energies of spin-purified, low-spin (LS) states according to eqn (4). Below, HS refers to the single-determinantal high-spin coupled state related to the low-spin state by spin flip(s) and $\langle S^2 \rangle$ is the expectation value of the total spin operator applied to the appropriate determinant. This broken-symmetry DFT approach has proven effective for the prediction of state-energy splittings in transition metal complexes.[40]

$$^{LS}E = \frac{^{BS}E(^{HS}\langle S^2 \rangle - ^{LS}\langle S^2 \rangle) - ^{HS}E(^{BS}\langle S^2 \rangle - ^{LS}\langle S^2 \rangle)}{^{HS}\langle S^2 \rangle - ^{BS}\langle S^2 \rangle} \quad (4)$$

Calculations of oxygen-18 kinetic isotope effects

Calculations of ^{18}O KIEs invoked Transition State Theory as formulated by Bigeleisen and Wolfsberg.[41] Once the transition state (TS) for a reaction was identified, using the DFT methods described above, a vibrational frequency analysis was performed. The change in normal and imaginary vibrational frequencies associated with the ^{16}O–^{16}O and ^{16}O–^{18}O producing species were analyzed.[19] All isotopic vibrations were considered and used without scaling or correction for anharmonicity to compute the ^{18}O KIE according to eqn (5). The terms representing the ^{18}O isotope effect on the reaction coordinate frequency ($^{18}\nu_{RC}$),[42,43] and the pseudo-equilibrium constant for attaining the TS from a specific precursor state ($^{18}K_{TS}$) are provided in the ESI.†

$$^{18}\text{O KIE} = {}^{18}\nu_{RC} \times {}^{18}K_{TS} \quad (5)$$

The calculation of ^{18}O KIEs relies on the ability of DFT to predict the mass-dependence of stable and imaginary vibrational modes of reactant and TS structures. The individual frequencies need not be computed accurately because the net isotopic shift of vibrations dictates the isotope effect. Equilibrium isotope effects on stable states have routinely been calculated from reduced partition function ratios (*i.e.* ^{18}O EIE = ZPE × EXC × MMI).[44] The terms correspond to the isotopic zero-point energy (ZPE), vibrational excitation energy (EXC) and mass and moments of inertia (MMI) of the reactant and product.[27a,45a] The $^{18}K_{TS}$ in eqn (5) is formulated analogously, except that one less ratio is present in the vibrational product term, VP, which is substituted for the MMI. The $^{18}\nu_{RC}$ term comes from the ratio of imaginary modes that define the reaction coordinate.[45] Apparently, $^{18}\nu_{RC}$ contributes a normal effect on reactions that involve O–O bond-making/breaking.[11,12b] When ^{18}O can adopt multiple positions during the reaction, ^{18}O KIEs calculated from Boltzmann-weighted populations are well approximated by simple averaging.
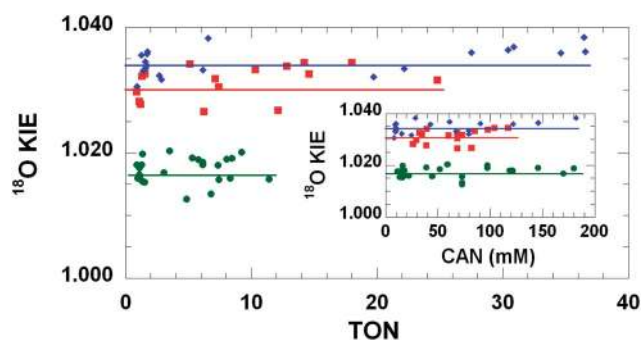

Fig. 3 Oxygen isotope fractionation determined from the analysis of O₂ according to eqn (2) at variable catalyst turnover number (TON) and CAN concentration (inset). Reactions were initiated by addition of **Ru** (red squares), **Ru₂**^{BD} (green circles) and **Ru₂**^{Hbpp} (blue diamonds) to acidic CAN solutions at 22 °C.

Discussion

Mechanisms considered

The competitive ^{18}O KIE is defined by the ratio of second order rate constants for forming the two most abundant oxygen isotopologues, ^{16,16}O₂ and ^{16,18}O₂. In the absence of complicating off-pathway H₂O exchange reactions with catalytic

intermediates, the ^{18}O KIE probes water oxidation mechanisms beginning with initial reversible coordination of H_2O to the reduced catalyst up to and including the first irreversible step.[42c] Transition states were calculated at two disparate levels of DFT (mPW and M06-L) to address the ^{18}O KIEs measured here. Irreversible O–O bonding changes during water attack/addition (**WA**) and oxo-coupling (**OC**) transition states are shown in Scheme 1. These reactions produce peroxo intermediates[46] that directly evolve O_2, hence giving rise to competitive ^{18}O KIEs.

The present investigation describes the first concurrent experimentally determined and DFT-calculated ^{18}O KIEs upon water oxidation under catalytic and stoichiometric conditions. In achieving this, moderately large normal ^{18}O KIEs have been determined and demonstrated to be consistent with O–O bond forming transition states. Importantly, these studies extend mechanistic understanding to the level of bonding changes.

The reaction sequences in Schemes 2–4 are shown to emphasize the questionable reversibility of oxidative steps that lead up to O–O bond formation. The exchangeability of H_2O within the catalytic initiator/resting reduced catalyst is implicit as is the H_2O exchangeability with oxidized ruthenium states formed prior to O–O bond formation. This is a fundamentally different scenario than that assumed in stoichiometric isotope tracer studies,[16a,17a,d,18c] wherein only one of the three catalytic systems examined (**Ru$_2^{Hbpp}$**)[18] readily gives interpretable results. **Ru** catalysis has been proposed to occur by a mechanism of **WA** at a ruthenyl site (Scheme 2).[21,49] Alternative mechanisms involving pre-association of CAN-derived species have been difficult to exclude, however.[16a,47] A somewhat different **WA** mechanism is formulated for **Ru$_2^{BD}$** initiated catalysis (Scheme 3), where the structure of the di-ruthenyl (V,V) intermediate facilitates proton transfer concomitant with O–O bond formation.[17,50] Two **OC** mechanisms via di-ruthenyl (IV,IV) and (IV,V) oxidations states are shown for **Ru$_2^{Hbpp}$** (Scheme 4).[18] This intramolecular pathway may result from structural constraints imposed by the bridging and meridional ligands.

Kinetics of water oxidation catalysis

In the catalytic reactions examined, rates of O_2 appearance depend linearly on the concentration of the ruthenium initiator.[19] Such observations argue against self-aggregation as the origin of the unusual sigmoidal kinetics observed with **Ru**. Although the catalytic rates appear first order in CAN at the

lowest concentrations analyzed, the linear phase is short and transitions to saturation differently than observed with **Ru$_2^{BD}$** or **Ru$_2^{Hbpp}$** (cf. Fig. 2). The sigmoid dependence on CAN observed during **Ru** catalysis suggests multimerization and/or coordination of a CAN-derived species, such as Ce^{IV}–OH, prior to catalyst oxidation. Despite the uncertain origin of this kinetic behavior, the invariance of ^{18}O KIE to CAN concentration suggests that the phenomenon does not affect the reaction transition state. A small inverse to negligible solvent deuterium isotope effect on the turnover rate constant measured under the same experimental conditions is inconclusive. A secondary isotope effect is possible as is a competing inverse isotope effect on pre-equilibrium H$^+$/D$^+$ transfer to the reactive ruthenyl species and a normal solvent kinetic isotope effect due to O–H/D bond cleavage concomitant with O–O bond formation.[23b]

The normal hyperbolic kinetics observed for catalysis involving the dimeric ruthenium complexes, **Ru$_2^{BD}$** and **Ru$_2^{Hbpp}$**, suggests that CAN interacts in a well-defined manner, avoiding coordination and/or aggregation. In the case of **Ru$_2^{BD}$**, the normal solvent deuterium isotope effect on k_{cat} is consistent with concerted O–H/D bond breaking and O–O bond formation in the **WA** transition state. At the other extreme, **Ru$_2^{Hbpp}$** shows no sign of a solvent isotope effect in perchloric acid or triflic acid, arguing against rate-limiting O–H/D transfer. The use of these acids with somewhat different pK_a values could expose variability if a competition between pre-equilibrium and primary kinetic isotope effects were responsible for the lack of solvent deuterium kinetic isotope effect.

The parameter k_{cat}, reflecting catalyst turnover at saturating levels of all substrates, increases in the order: **Ru** < **Ru$_2^{Hbpp}$** < **Ru$_2^{BD}$**. A similar trend, with a more significant diminution observed with **Ru** characterizes k_{cat}/K_{CAN}. This parameter probes all steps beginning with CAN association, leading up to and including the first irreversible step, which could involve O–O bond formation.[21] By definition, k_{cat} is determined by unimolecular steps such as O–O bond formation and/or O_2 release. It is, therefore, possible that the two kinetic parameters are controlled by the same irreversible O–O bond-forming step. This possibility is consistent with the observed ^{18}O KIEs considered in the following section.

## Interpretation of competitive oxygen-18 kinetic isotope effects

The ^{18}O KIEs for **Ru** and **Ru$_2^{BD}$** measured in strongly acidic media with CAN as the sacrificial oxidant ($E^{\circ\prime}$ ~1.6 V vs. NHE) are two to three times larger than those determined in neutral solutions using photo-generated [Ru^{III}(bpy)$_3$]$^{3+}$ ($E^{\circ\prime}$ ~1.2 V vs. NHE) in 0.05 M KP$_i$ as the oxidant. This change in ^{18}O KIE with pH implicates a change in the nature of the TS, and possibly the identity of the first irreversible step. Lowering $E^{\circ\prime}$ of the oxidant disfavors formation of the reactive Ru=O intermediate and would be expected to change the highest energy TS such that the ^{18}O KIE is significantly diminished from the large normal values anticipated for O–O bond formation. Another possibility is that phosphate buffer facilitates proton removal[10] upon **WA**, changing the TS for O–O bond formation from that in non-coordinating media.
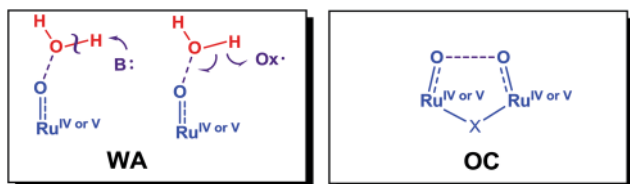
Scheme 1 Transition states corresponding to water attack/addition (**WA**) and oxo-coupling (**OC**).
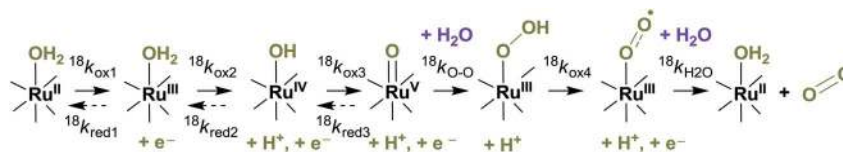
Scheme 2   Minimal mechanism proposed for Ru-initiated water oxidation.
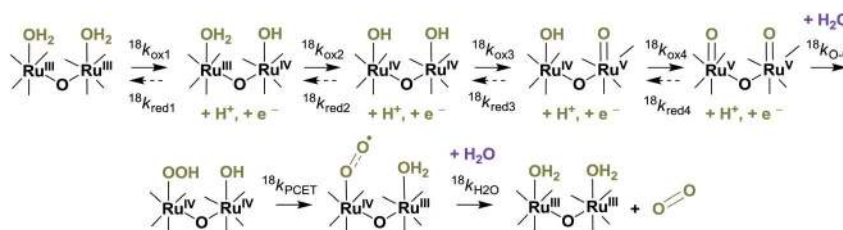
Scheme 3   Minimal mechanism proposed for Ru_2^{BD}-initiated water oxidation.
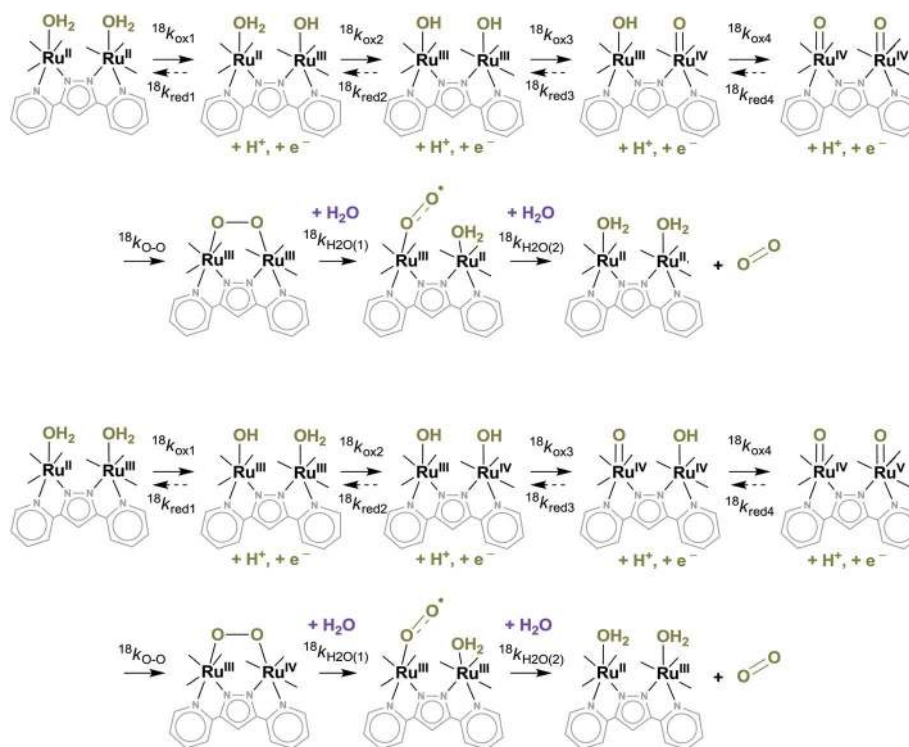
Scheme 4   Minimal mechanisms proposed for Ru_2^{Hbpp}-initiated water oxidation via intermediates in the +IV,+IV or +IV,+V oxidation states.

Calculation of all possible reaction coordinates leading to water oxidation is beyond the scope of the present investigations, however, experimental ^{18}O KIEs are available for specific steps. For instance, Taube et al. measured a competitive equilibrium effect on H_2O coordination to an inert cobalt(III) ion exposing a surprisingly large $^{18}K_{H_2O}$ of ~1.019.[48] The $^{18}K_{H_2O}$ is viewed as an upper limit to $^{18}k_{H_2O}$ by analogy with O_2 activation by reduced transition metals.[12] Oxidation of a ruthenium(II) aqua complex is expected to exhibit an inverse $^{18}K_{ox}$ due to strengthening of bonding within the product relative to the reactant and a $^{18}k_{ox}$ on electron transfer ca. 1.010 based on

measurements by McLendon et al. and calculations by Jortner et al. on outer-sphere electron transfer.[49] More recent studies suggest that $^{18}k_{ox}$ is closer to unity for a proton-coupled electron transfer.[50]

The competitive ^{18}O KIE on catalytic water oxidation catalysis is determined from the O_2 produced from natural abundance water. As a result, this parameter is capable of probing all steps beginning with coordination of H_2O to the reduced catalyst and culminating in O–O bond formation (Schemes 2–4). Assuming no interference from off-pathway exchange, the ^{18}O KIE(H_2O) is defined by eqn (6), which is the product of pre-

equilibrium isotope effects ($^{18}K_{H_2O} \times {}^{18}K_{ox}$) and the kinetic isotope effect on O–O bond-formation ($^{18}k_{O-O}$). In contrast, if all steps in the mechanisms were irreversible, the competitive ^{18}O KIEs would be defined by eqn (7) or eqn (8), reflecting only those steps that consume H_2O. Eqn (7) represents catalysis by **WA**, as proposed for **Ru** and $\mathbf{Ru_2^{BD}}$, where the ^{18}O KIE is the average of the microscopic $^{18}k_{O-O}$ due to **WA** and k_{H_2O} for displacement of O_2 by H_2O. Eqn (8) applies to catalysis by **OC** as proposed for $\mathbf{Ru_2^{Hbpp}}$. In this case, $^{18}k_{O-O}$ is masked by irreversible H_2O coordination in two distinct steps. In contrast, all steps following irreversible O–O bond-formation are masked in eqn (6).

$$^{18}O\ KIE(H_2O) = {}^{18}K_{H_2O} \times {}^{18}K_{ox} \times {}^{18}k_{O-O} \quad (6)$$

$$^{18}O\ KIE(H_2O) = \tfrac{1}{2}({}^{18}k_{O-O} + {}^{18}k_{H_2O}) \quad (7)$$

$$^{18}O\ KIE(H_2O) = \tfrac{1}{2}({}^{18}k_{H_2O(1)} + {}^{18}k_{H_2O(2)}) \quad (8)$$

The ^{18}O KIEs shown in Fig. 3 are the same at highly variable concentrations of CAN and under single and multi-turnover acidic conditions. These results point to a common (O_2) product-determining step. The CAN independence suggests the same irreversible step at low concentrations and high concentrations, as indicated by k_{cat}/K_{CAN} and k_{cat}, respectively. That the same isotope fractionation is observed for the single turnover and for multi-turnover reactions extends results of earlier isotope tracer studies to the catalytic mechanism. Finally, the experimental ^{18}O KIEs agree with ^{18}O KIEs calculated for specific transition states.[18c,51,52]

The interpretation of ^{18}O KIEs summarized in Table 2 is not without some ambiguity, however. It is possible that reversible coordination of water followed by oxidation of the reduced ruthenium intermediate could coincidentally give rise to the same ^{18}O KIE(H_2O) defined as the product ($^{18}K_{H_2O} \times {}^{18}k_{ox}$). In addition, off-pathway H_2O exchange following the aforementioned irreversible oxidation step could wash out any isotope fractionation but, as long as O–O bond formation is irreversible, the $^{18}k_{O-O}$ would be expressed in the O_2 produced. Incidentally, $^{18}k_{O-O}$ is similar to the ^{18}O KIE(H_2O) calculated from eqn (6), making the pre-equilibrium isotope effect on conversion of H_2O to a reactive Ru=O intermediate near unity.

Contribution to the ^{18}O KIE from O_2 loss is unlikely given the apparently irreversible nature of O–O bond formation. Evaluation of the ground state thermodynamics supports this view,

placing the Ru–O_2 adduct at much lower energy than the reactive Ru=O intermediate that undergoes O–O bond formation. Thus the barrier to O_2 loss is expected to be insignificant.[21] Furthermore, all studies carried out to date suggest that simple O_2 dissociation is characterized by inverse ^{18}O KIEs approaching unity.[12,53]

Transition states in water oxidation catalysis are more likely to involve the displacement of O_2 by H_2O than simple dissociation, as observed in polar organic solvents. Such a TS for an O_2 displacement reaction that regenerates $\mathbf{Ru_2^{Hbpp}}$ has been identified,[18c] requiring multiple explicit H_2O molecules in a hydrogen-bonded configuration. Though the ^{18}O KIE(H_2O) was calculated to be indistinguishable from unity, further investigations are needed to understand the range of possible isotope effects. As described below for **WA**, multiple configurations of explicit water molecules can result in ^{18}O KIEs spanning a wide range. Evolution of O_2 may be similar in this respect.

Transition states for O–O bond formation

Three **WA** TSs involving four or five explicit H_2O molecules in multiple hydrogen bond configurations were identified for catalytic oxidation initiated by **Ru** (Fig. 4). At both the *m*PW and M06-L levels of theory, $\mathbf{WA^{4a}}$ exhibited the most "product-like" structure relative to the other TSs of comparable energy. The Ru–O bond lengthens from 1.688 Å in the Ru^V=O precursor to 1.875 Å in $\mathbf{WA^{4a}}$ as the O–O bond distance contracts to 1.590 Å. These changes are significantly larger than those observed for $\mathbf{WA^{4b}}$ and $\mathbf{WA^5}$ where the Ru–O bond distance expands to 1.747 Å and 1.743 Å, respectively, and the O–O bond distance contracts to 1.962 Å in $\mathbf{WA^{4b}}$ and 1.974 Å in $\mathbf{WA^5}$.

Despite differences in the bonding changes, the calculated free energy barriers, $\Delta G^{\ddagger}$(O–O), fall within a narrow range from 19 to 23 kcal mol^{-1} and are close to the experimental estimate of 18.9 kcal mol^{-1}. The measured ^{18}O KIE can be reproduced using two disparate DFT methods; the results are given in parentheses. The $^{18}k_{O-O}$ associated with the most product-like TS, $\mathbf{WA^{4a}}$, ranges from 1.0240 (*m*PW) to 1.0303 (M06-L). Similarly, the ^{18}O KIE(H_2O), defined according to eqn (6) for the reaction beginning with H_2O and proceeding *via* a sequence of reversible steps, leading up to and including **WA**, ranges from 1.0225 (*m*PW) to 1.0260 (M06-L). Application of a solvent correction to the gas phase values results in an insignificant change. This

Table 2 Comparison of measured ^{18}O KIEs to those calculated for irreversible O−O bond formation. The range for the proposed transition state is given by the results of two DFT methods: *m*PW/M06-L

Initiator	^{18}O KIE $(\pm 1\sigma)^a$	Proposed TS^b	$^{18}k_{O-O}{}^c$	^{18}O KIE(H_2O) (eqn (6))
Ru	1.0313 ± 0.0027	$^2WA^{4a}$	1.0240/1.0303	1.0225/1.0260
Ru_2^{BD}	1.0172 ± 0.0020	$^1WA^2$	1.0151/1.0172	1.0167/1.0170
Ru_2^{Hbpp}	1.0346 ± 0.0021	^1OC	$1.0311/1.0447^d$	$1.0385/1.0504^d$

^{a} Experimental value derived from eqn (2). Solving eqn (3) indicates **Ru** (1.0306 ± 0.0004), $\mathbf{Ru_2^{BD}}$ (1.0169 ± 0.0003) and $\mathbf{Ru_2^{Hbpp}}$ (1.0347 ± 0.0004). ^{b} Defined in Fig. 4–6 where the left superscript refers to the spin state and the right subscript refers to the number and configuration of explicit H_2O molecules used in the calculation. ^{c} Full computational details, including results for alternative H_2O configurations, solvation states and spin states are provided in the ESI.† ^{d} For the reactions *via* the di-ruthenyl (IV,IV) oxidation state. M06-L calculations indicate the di-ruthenyl intermediate in (IV,V) oxidation state reacts *via* a ^2OC TS with $^{18}k_{O-O} = 1.0445$ and ^{18}O KIE(H_2O) = 1.0480 for comparison.
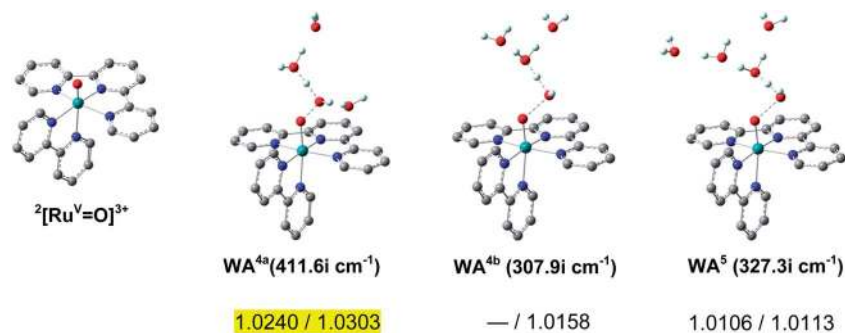
Fig. 4 Precursor and transition states for catalytic water oxidation initiated by Ru at the M06-L level of theory. Imaginary frequencies of the light TS isotopologues are shown (bold) and the range of calculated $^{18}k_{O-O}$ is also provided for calculations using (mPW/M06-L).

insensitivity can be explained by the observation that while calculated vibrational frequencies are medium-dependent, the mass-dependence that gives the isotope shift is not.

The blue dimer, $\mathbf{Ru_2^{BD}}$,[54] is converted into di-ruthenyl intermediates that exist in (IV,V) and (V,V) oxidation states during catalysis.[55,56] DFT calculations were undertaken for reactions of the (V,V) intermediate in an unrestricted singlet state assuming weak anti-ferromagnetic coupling between formally $Ru^V{=}O$ units with doublet electronic structures.[57] In contrast to results from ^{18}O tracer studies,[17a,d] the competitive ^{18}O KIEs seem to suggest reactivity by a single mechanism. Two distinct water attack TSs, $\mathbf{WA^1}$ and $\mathbf{WA^2}$, featuring one or two explicit hydrogen-bonded H_2O molecules, were identified and compared to a new TS for $\mathbf{OC}$ identified at the M06-L level of theory (Fig. 5). The most product-like TS, defined above by extension of the Ru–O bond and contraction of the O–O bond, is designated $\mathbf{^1WA^2}$. A staggered precursor to this species was identified with a Ru–O bond length of 1.723 Å and O–O distance of 5.112 Å. In the $\mathbf{^1WA^2}$ TS, the Ru–OO bond length expands to 1.931 Å and the O–O bond distance contracts to 1.569 Å. The alternative $\mathbf{^1OC}$ TS is characterized by Ru–OO and O–O bond distances of 1.807–1.816 Å and 1.720 Å. Likewise, $\mathbf{^1WA^1}$ exhibits Ru–OO and O–O bond distances of 1.782 and 1.801 Å, respectively.

Bonding changes similar to those associated with $\mathbf{^1WA^2}$ are observed for the triplet state, $\mathbf{^3WA^2}$. In this case, the precursor has an eclipsed conformation, where the Ru–O bond lengths are 1.764 Å and 1.697 Å and the O–O distance is 2.827 Å. In the most product-like $\mathbf{^3WA^2}$ TS, the Ru–OO bond length is 1.935 Å and the O–O bond length is 1.560 Å. The associated vibrational

changes result in computed ^{18}O KIEs that are remarkably similar to those computed for $\mathbf{^1WA^2}$ despite major differences in the precursor structure.[19]

For $\mathbf{^1WA^2}$, the calculated $\Delta G^{\ddagger}(O{-}O) \cong 36.5$ kcal mol^{-1} is mid range compared to the other TSs. A smaller $\Delta G^{\ddagger}(O{-}O)$ was calculated for a previously unidentified oxo-coupling TS in either the unrestricted singlet state, $\mathbf{^1OC}$ ($\cong 27.3$ kcal mol^{-1}) or triplet state $\mathbf{^3OC}$ ($\cong 27.0$ kcal mol^{-1}). Interestingly, this is the only case where the same TS could not also be identified using the mPW functional. $\Delta G^{\ddagger}(O{-}O)$ for the transition state involving a single H_2O, $\mathbf{^1WA^1}$ ($\cong 46.8$ kcal mol^{-1}), is energetically disfavored, consistent with other computational findings.[52]

In contrast to the calculated $\Delta G^{\ddagger}(O{-}O)$, which deviates significantly from the measured value in one out of three cases, the isotope effect calculated for the TS with the most product-like character routinely agrees with the measured ^{18}O KIE. The $\mathbf{^1WA^2}$ reaction of $\mathbf{Ru_2^{BD}}$ modeled in the gas phase is characterized by $^{18}k_{O-O}$ values of 1.0151 (mPW) and 1.0172 (M06-L), which are within experimental error of the measured competitive ^{18}O KIE. For the same TS, the ^{18}O KIE(H_2O) values, computed using eqn (6) are 1.0167 (mPW) and 1.0170 (M06-L). The analogous calculations on the triplet TS, $\mathbf{^3WA^2}$, are essentially indistinguishable from those above, with $^{18}k_{O-O}$ equal to 1.0146 (M06-L) and ^{18}O KIE(H_2O) equal to 1.0158 (M06-L). Insignificant variation was detectable for isotope effects calculated along unrestricted singlet, triplet or quintet surfaces and following re-optimization of structures within a continuum solvation model.[19]

Catalysis initiated by the geometrically constrained di-ruthenium (II,II) complex, $\mathbf{Ru_2^{Hbpp}}$, is considered to occur *via*
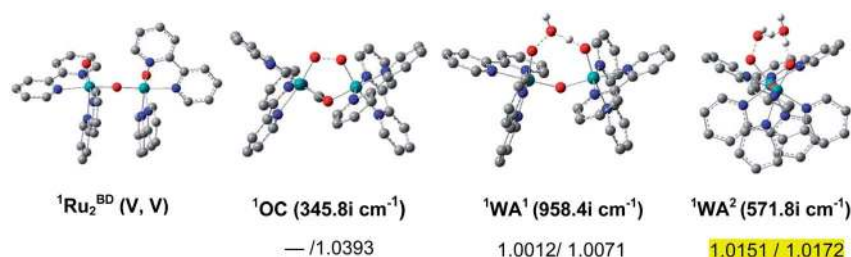

Fig. 5 Precursor and transition states for catalytic water oxidation initiated by $\mathbf{Ru_2^{BD}}$ at the M06-L level of theory. Imaginary frequencies of the light TS isotopologues are shown (bold) and the range of calculated $^{18}k_{O-O}$ is also provided for calculations using (mPW/M06-L).

two different oxidized precursor states (Fig. 6). DFT calculations were undertaken to model the O–O bond forming reactions of di-ruthenyl intermediates in the (IV,IV) and (IV,V) oxidation states. No significant deviations in the ^{18}O KIEs were observed for reactions in high-spin and low-spin states. The TS structures for **OC**, **WA^1** and **WA^2** were associated with unique isotope effects. Similar to the calculations above for **Ru** and **Ru$_2^{BD}$**, the most advanced TSs are associated with ^{18}O KIEs that exhibit the best agreement with experimental measurements on **Ru$_2^{Hbpp}$**.

Consistent with the absence of solvent deuterium isotope effects on k_{cat} and the results of ^{18}O tracer studies,[18c] the ^{18}O KIEs computed implicate **OC**. Out of all mechanisms examined, the most product-like TS for the reaction of the di-ruthenyl (IV,IV) intermediate in the unrestricted singlet state (**^{1}OC**) involves elongation of the Ru–O bond from 1.757 Å to 1.840 Å and contraction of the O–O bond distance to 1.715 Å. **^{1}WA^1** and **^{1}WA^2** exhibited Ru–O and O–O bond distances of 1.760 and 1.984 Å and 1.769 and 1.977 Å, respectively. Somewhat different behavior characterizes reaction of the diruthenyl (IV, V) intermediate in the low-spin doublet state (**^{2}OC**) where the precursor Ru–O bonds elongate from 1.724 Å and 1.767 Å to 1.808 Å and the O–O bond distance in the TS contracts to 1.691 Å. Here **^{2}WA^1** exhibits Ru–O and O–O bond distances of 1.789 and 1.749 Å and **^{2}WA^2** exhibits 1.860 and 1.612 Å, respectively. Reaction *via* a **^{2}WA^2** mechanism is, however, inconsistent with the absence of a solvent deuterium kinetic isotope effect.

The **OC** TSs are substantially lower in energy than those associated with **WA^1** and **WA^2** mechanisms. The $\Delta G^{\ddagger}$(O–O) corresponding to **^{1}OC** is ~14 kcal mol^{-1} while the **^{1}WA^1** and **^{1}WA^2** calculated from the di-ruthenium (IV,IV) bis-oxo intermediate are 25–40 kcal mol^{-1} higher in energy.[19] The ^{18}O KIEs predicted for **WA** mechanisms are too small to be reconciled with the experimental results in this case. The di-ruthenium (IV,V) bis-oxo intermediate is expected to react *via* **OC** where

$\Delta G^{\ddagger}$(O–O) for **^{2}OC** is ~14 kcal mol^{-1} and the **^{2}WA^1** and **^{2}WA^2** are *ca.* 10 kcal mol^{-1} higher in energy.

The calculated ^{18}O isotope effects for the most product-like TSs coincide with the **OC** mechanism proposed for stoichiometric oxidation by **Ru$_2^{Hbpp}$**.[18] The $^{18}k_{O-O}$ associated with the di-ruthenium (IV,IV) bis-oxo intermediate is predicted to be between 1.0311 (*m*PW) and 1.0447 (M06-L); while the ^{18}O KIE(H$_2$O) computed using eqn (6) ranges from 1.0385 (*m*PW) to 1.0504 (M06-L). Starting from the di-ruthenium (IV,V) bis-oxo intermediate, $^{18}k_{O-O}$ is predicted to be 1.0445 (M06-L) and the ^{18}O KIE(H$_2$O) is predicted to be 1.0480 (M06-L). Reactions *via* the same intermediate in the quartet spin state span a comparable range of isotope effects and $\Delta G^{\ddagger}$(O–O).[19] As mentioned above, the calculated isotope effects for **Ru$_2^{Hbpp}$** are insensitive to spin-state as well as added solvent corrections.[19]

In summary, DFT affords vibrational frequencies used without scaling or correction for anharmonicity to calculate isotope effects that span distinct ranges. For **WA** at a reactive Ru^V=O intermediate, $^{18}k_{O-O}$ and KIE(H$_2$O) formulated according to eqn (6), ranges from ~1.00 to 1.03. The analogous effects calculated for **OC** are larger, varying from ~1.03 to 1.050. Although these results seem promising, subtle differences resulting from the number of explicit H$_2$O considered in **WA** calculations can have unforeseen effects. Therefore, caution should used when interpreting competitive ^{18}O KIEs in the absence of supporting mechanistic data.

The small overlap in the ranges of isotope effects associated with the **OC** and **WA** mechanisms is unsurprising because the oxygen nuclei have disparate roles. According to Scheme S2,†[19] the $^{18}k_{O-O}$ computed for **WA** considers the two cases: (i) where ^{18}O is positioned on the attacking H$_2$O and (ii) where ^{18}O is bonded directly to the electrophilic Ru=O. In **Ru**-initiated catalysis, the calculated $^{18}k_{O-O}$ for the **WA^{4a}** TSs corresponding to (i) and (ii) are 1.0089 and 1.0402, respectively, revealing
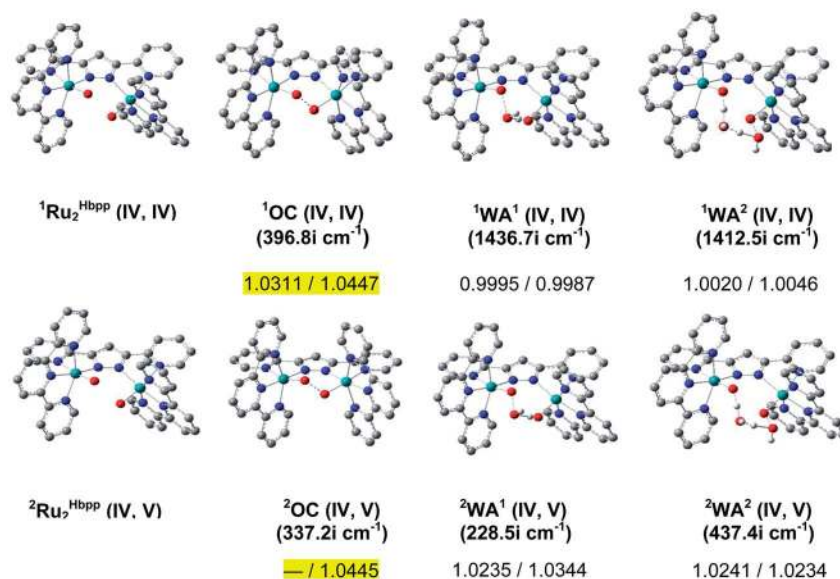

Fig. 6 Precursor and transition states for catalytic water oxidation initiated by **Ru$_2^{Hbpp}$** at the M06-L level of theory. Imaginary frequencies of the light TS isotopologues are shown (bold) and the range of calculated $^{18}k_{O-O}$ is also provided for calculations using (*m*PW/M06-L).

differences in the vibrational frequency changes that characterize O–O bond-making coupled to O–H bond-breaking.[19] Application of Boltzmann-weighting for the positional preference of ^{18}O results in $^{18}k_{O-O} = 1.0240$, which is only slightly different from the average $^{18}k_{O-O} = 1.0245$. No such considerations are necessary for the symmetric **OC** reactions.

Implications for oxygenic photosynthesis

During photosynthesis, visible photons generate a transient charge-separated state that oxidizes chlorophyll P680. The P680[•+] intermediate formed has a high redox potential ($E° \cong 1.3$ V *vs.* NHE) that facilitates formation of a tyrosyl radical ($Y_z^{•}$, $E° \cong 1.2$ V *vs.* NHE) that is kinetically and thermodynamically competent to oxidize H_2O bound to manganese in the oxygen-evolving complex (OEC).[1] A number of competitive isotope fractionation studies at natural abundance have indicated ^{18}O KIEs from inverse to unity for water oxidation by PSII, using the same experimental approach described in the present study.[13,14]

Two simple assumptions allow for an interpretation of the slightly inverse ^{18}O KIE associated with PSII catalysis.[13a] First, all steps during water oxidation catalysis must be kinetically irreversible. Second, the ^{18}O KIE must be uninfluenced by processes that reductively consume O_2 at the same time it is produced. In this case, eqn (7) predicts that O–O bond formation by **WA** upon the reactive manganyl intermediate ($Mn^V=O$ or $Mn^{IV}=O^{•}$)[58] should give rise to a competitive ^{18}O KIE somewhat greater than unity. Yet if the same intermediate state of the OEC reacts by **OC**, as defined by eqn (8), two H_2O coordination steps give rise to the competitive ^{18}O KIE, possibly accounting for the accepted value near unity.[13a] Spectroscopic studies at variable O_2 pressures have attempted to test for a Mn–O_2 intermediate.[59] Yet the accumulation of this species is not expected unless O–O bond formation is rapid and reversible prior to O_2 release. While this situation is possible,[12b] it seems unlikely in view of the results presented here.

Conclusions

Three major findings have emerged from this study. (1) Competitive ^{18}O KIEs derived from the analysis of O_2 under catalytic conditions are the same under stoichiometric conditions, where off-pathway exchange *via* oxidized ruthenium intermediates does not occur.[17a,17d,18c] (2) Variable concentrations of ceric ammonium nitrate do not affect the ^{18}O KIEs, implicating a common (O_2) product-forming step, without assistance from the sacrificial oxidant or its derivatives. In addition, the results are consistent with k_{cat} and k_{cat}/K_{CAN} being limited irreversible O–O bond formation. (3) Kinetic isotope effects were calculated using Transition State Theory and DFT to provide the full set of imaginary and normal vibrations without scaling or correction for anharmonicity. The computed results agreed with the moderately large normal measured ^{18}O KIEs when the transition states identified were the most "product-like" of all those considered. Furthermore, the proposed transition states were corroborated by steady-state kinetic results and earlier isotope tracer studies.

Competitive ^{18}O KIEs are useful in identifying O–O bond-forming mechanisms of water oxidation catalysis. The results support "solvent-assisted" water attack as the transition state for catalysis initiated by the monomeric **Ru**. In catalysis initiated by Ru_2^{BD}, intramolecular reactivity is facile and appears to involve an internally hydrogen-bonded water attack/addition transition state. In contrast, Ru_2^{Hbpp} reacts by oxo-coupling, possibly because of geometric constraints imposed by the ligand set. These results extend those determined for stoichiometric reactions to mechanisms of catalysis while providing visualization of the changes in bond vibrations.

Experimental

All chemicals were obtained commercially in the highest purity available and used as received. $RuCl_3·nH_2O$ was obtained from Pressure Chemicals. Hexamethyldisiloxane (HMDS) was obtained from Lancaster. Ceric ammonium nitrate (CAN), hexamethylphosphoramide (HMPA), 2,2′-bipyridine (bpy), 2,2′; 6′,2″-terpyridine (tpy), sodium triflate (NaOTf), lithium perchlorate ($LiClO_4$), sodium perchlorate ($NaClO_4$) and potassium persulfate ($K_2S_2O_8$) were obtained from Sigma-Aldrich. All deuterated solvents were purchased from Cambridge Isotope Laboratories. Unlabeled water was purified to 18 MΩ by passing through a Millipore ultra-filtration system.

NMR spectra were recorded on a 400 MHz Bruker Avance spectrometer at ambient temperature. Chemical shifts were referenced to the residual protio impurities in the deuterated solvent. Ruthenium complexes were dissolved in deuterated solvents (d_6-DMSO, d_6-acetone or d_3-MeOD) and quantified relative to an internal standard. Electronic absorption spectra were recorded on an Agilent 8453 UV-Vis spectrophotometer. Elemental analyses were performed by Atlantic Microlabs Norcross, GA. Initial rates of O_2 production were measured using a Clark-type oxygen electrode (Yellow Springs Inc.; 5300A voltmeter and 5331A probe) inside a water-jacketed chamber at 22 ± 0.2 °C. Composition of the gaseous phase was also confirmed to be made up of O_2 determined by online mass-spectrometry with an OmniStar GSD 301 C (Pfeiffer) quadrupole mass-spectrometer.[18]

$[Ru(tpy)(bpy)(H_2O)](ClO_4)_2$ (**Ru**), cis,cis-$[(Ru(bpy)_2(H_2O))_2(\mu$-O)]$(ClO_4)_4$ (Ru_2^{BD}), and $\{[Ru(tpy)]_2(\mu$-bpp)$(\mu$-OAc)$\}(ClO_4)_2$ (Ru_2^{Hbpp}) were synthesized in milligram quantities and handled with a rubber tipped spatula. (**Caution!** *Perchlorate salts are potentially explosive and should be handled according to accepted safety guidelines*).[20] Analytic purity was gauged to be >95% for complexes used in experiments. Electronic absorption was used to determine the following extinction coefficients: **Ru** ($\varepsilon_{475nm} = 9000 \pm 300$ M^{-1} cm^{-1}), Ru_2^{BD} ($\varepsilon_{638nm} = 22000 \pm 260$ M^{-1} cm^{-1}), and Ru_2^{Hbpp} ε_{471nm} (12580 $\pm$ 1780 M^{-1} cm^{-1}). The results were corroborated by quantitative ^1H-NMR spectroscopy[19] and elemental analysis. The following data were obtained for $[Ru(tpy)(bpy)(H_2O)](ClO_4)_2$: calc.: C, 42.44; H, 2.99; N, 9.90. Found: C, 42.16; H, 2.76; N, 9.77; cis,cis-$[(Ru(bpy)_2(H_2O))_2(\mu$-O)]$(ClO_4)_4·H_2O$ calc.: C, 37.11; H, 2.96; N, 8.65. Found: C, 37.02; H, 2.92; N, 8.75; and $\{[Ru(tpy)]_2(\mu$-bpp)$(\mu$-OAc)$\}(ClO_4)_2·H_2O$ calc.: C, 46.36; H, 3.11; N, 12.01. Found: C, 46.13; H, 3.12; N, 11.69.

Acknowledgements

References

1 J. P. McEvoy and G. W. Brudvig, *Chem. Rev.*, 2006, **106**, 4455.

2 (*a*) J. J. Concepcion, J. W. Jurss, M. K. Brennaman, P. G. Hoertz, M. K. O. Patrocinio, N. Y. M. Iha, J. L. Templeton and T. J. Meyer, *Acc. Chem. Res.*, 2009, **42**, 1954; (*b*) D. J. Wasylenko, R. D. Palmer and C. P. Berlinguette, *Chem. Commun.*, 2013, **49**, 218; (*c*) A. E. Clark and J. K. Hurst, *Prog. Inorg. Chem.*, 2012, **57**, 1; (*d*) M.-Y. Ghosh Baik, *Angew. Chem.*, 2012, **51**, 1221; (*e*) Y. Xu, A. Fischer, L. Duan, L. Tong, E. Gabrielsson, B. Aakermark and L. Sun, *Angew. Chem.*, 2010, **49**, 8934; (*f*) R. Zong and R. P. Thummel, *J. Am. Chem. Soc.*, 2005, **127**, 12802.

3 (*a*) M. Calvin, *Acc. Chem. Res.*, 1978, **10**, 369; (*b*) A. , Magnuson, M. Anderlund, O. Johansson, P. Lindblad, R. Lomoth, T. Polivka, S. Ott, K. Stensjö, S. Styring, V. Sundström and L. Hammarström, *Acc. Chem. Res.*, 2009, **42**, 1899.

4 (*a*) P. D. Frischmann, K. Mahata and F. Wuerthner, *Chem. Soc. Rev.*, 2013, **42**, 1847; (*b*) V. Balzani, A. Credi and M. Venturi, *Curr. Opin. Chem. Biol.*, 1997, **1**, 506; (*c*) D. Gust, T. A. Moore and A. L. Moore, *Acc. Chem. Res.*, 2009, **42**, 1890.

5 N. S. Lewis and D. G. Nocera, *Proc. Natl. Acad. Sci. U. S. A.*, 2006, **103**, 15729.

6 M. G. Walter, E. L. Warren, J. R. McKone, S. W. Boettcher, Q. Mi, E. A. Santori and N. S. Lewis, *Chem. Rev.*, 2010, **110**, 6446–6473.

7 (*a*) P. M. Cox, R. A. Betts, C. D. Jones, S. A. Spall and L. J. Totterdell, *Nature*, 2000, **408**, 184; (*b*) A. J. Weaver and C. Hillaire-Marcel, *Science*, 2004, **304**, 400; (*c*) J. Hansen, M. Sato, R. Ruedy, K. Lo, D. W. Lea and M. Medina-Elizade, *Proc. Natl. Acad. Sci. U. S. A.*, 2006, **103**, 14288.

8 J. O. 'M. Bockris, *Int. J. Hydrogen Energy*, 2002, **27**, 731.

9 (*a*) X. Liu and F. Wang, *Coord. Chem. Rev.*, 2012, **256**, 1115; (*b*) X. Sala, I. Romero, M. Rodriguez, L. Escriche and A. Llobet, *Angew. Chem., Int. Ed.*, 2009, **48**, 2842; (*c*) G. C. Dismukes, R. Brimblecombe, G. A. N. Felton, R. S. Pryadun, J. E. Sheats, L. Spiccia and G. F. Swiegers, *Acc. Chem. Res.*, 2009, **42**, 1935–1943; (*d*) W. Ruttinger and G. C. Dismukes, *Chem. Rev.*, 1997, **97**, 1.

10 M. H. V. Huynh and T. J. Meyer, *Chem. Rev.*, 2007, **107**, 5004.

11 R. Sarma, A. M. Angeles-Boza, D. W. Brinkley and J. P. Roth, *J. Am. Chem. Soc.*, 2012, **134**, 15371.

12 (*a*) J. P. Roth, *Acc. Chem. Res.*, 2009, **42**, 399; (*b*) D. C. Ashley and D. W. Brinkley, *Inorg. Chem.*, 2010, **49**, 3661.

13 (*a*) R. D. Guy, M. L. Fogel and J. A. Berry, *Plant Physiol.*, 1993, **101**, 37; (*b*) K. Burda, K. P. Bader and G. H. Schmid, *Biochim. Biophys. Acta*, 2003, **1557**, 77; (*c*) H. Metzner, K. Fischer and O. Bazlen, *Biochim. Biophys. Acta, Bioenerg.*, 1979, **548**, 287.

14 (*a*) D. Eisenstadt, E. Barkan, B. Luz and A. Kaplan, *Photosynt. Res.*, 2010, **103**, 97; (*b*) G. Tcherkez and G. D. Farquhar, *Funct. Plant Biol.*, 2007, **34**, 1049.

15 (*a*) M. Dole and G. Jenks, *Science*, 1944, **100**, 409; (*b*) M. D. Kamen and H. A. Barker, *Proc. Natl. Acad. Sci. U. S. A.*, 1945, **31**, 8; (*c*) B. Luz, E. Barkan, M. L. Bender, M. H. Thiemens and K. A. Boering, *Nature*, 1999, **400**, 547.

16 (*a*) D. J. Wasylenko, C. Ganesamoorthy, B. D. Koivisto, M. A. Henderson, H. D. Osthoff and C. P. Berlinguette, *J. Am. Chem. Soc.*, 2010, **132**, 16094; (*b*) S. Masaoka and K. Sakai, *Chem. Lett.*, 2009, **38**, 182; (*c*) D. J. Wasylenko, C. Ganesamoorthy, M. A. Henderson and C. P. Berlinguette, *Inorg. Chem.*, 2011, **50**, 3622; (*d*) D. J. Wasylenko, C. Ganesamoorthy, B. D. Koivisto, M. A. Henderson and C. P. Berlinguette, *Inorg. Chem.*, 2010, **29**, 2202.

17 (*a*) J. L. Cape, W. F. Siems, J. K. Hurst, J. L. Cape, S. V. Lymar, T. Lightbody and J. K. Hurst, *Inorg. Chem.*, 2009, **48**, 8729; (*b*) H. Hamada, W. F. Siems, T. Koike and J. K. Hurst, *J. Am. Chem. Soc.*, 2004, **126**, 9786; (*c*) R. A. Binstead, C. W. Chronister, J. Ni, C. M. Hartshorn and T. J. Meyer, *J. Am. Chem. Soc.*, 2000, **122**, 8464; (*d*) D. A. Geselowitz and T. J. Meyer, *Inorg. Chem.*, 1990, **29**, 3894.

18 (*a*) C. Sens, I. Romero, M. Rodriguez, A. Llobet, T. Parella and J. Benet-Buchholz, *J. Am. Chem. Soc.*, 2004, **126**, 7798; (*b*) S. Romain, F. Bozoglian, X. Sala and A. Llobet, *J. Am. Chem. Soc.*, 2009, **131**, 2768; (*c*) F. Bozoglian, S. Romain, M. Z. Ertem, T. K. Todorova, C. Sens, J. Mola, M. Rodrıguez, I. Romero, J. Benet-Buchholz, X. Fontrodona, C. J. Cramer, L. Gagliardi and A. Llobet, *J. Am. Chem. Soc.*, 2009, **131**, 15176.

19 ESI.†

20 S. K. Mendiratta, R. L. Dotson and R. T. Brooker, *Kirk-Othmer Encyclopedia of Chemical Technology*, ed. A. Seidel, 5th edn, 2006, vol. 18, p. 274.

21 A. M. Angeles-Boza and J. P. Roth, *Inorg. Chem.*, 2012, **51**, 4722.

22 K. Binnemans, in *Handbook on Physics and Chemistry of Rare Earths*, ed. K. A. Gschneidner Jr, J-C. G. Bünzli and V. K. Pacharsky, Elsevier, London, England 2006, vol. 36.

23 (*a*) D. Moonshiram, V. Purohit, J. J. Concepcion, T. J. Meyer and Y. Pushkar, *Materials*, 2013, **6**, 392; (*b*) Z. Chen, J. J. Concepcion, Q. Hu, W. Yang, P. G. Hoertz and T. J. Meyer, *Proc. Natl. Acad. Sci. U. S. A.*, 2010, **107**, 7225.

24 (*a*) J. L. Cape, F. Siems and J. K. Hurst, *Inorg. Chem.*, 2009, **48**, 9729; (*b*) P. Ghosh, B. S. Brunschwig, M. H. Chou, C. Creutz and N. Sutin, *J. Am. Chem. Soc.*, 1984, **106**, 4772; (*c*) S. W. Gersten, G. J. Samuels and T. J. Meyer, *J. Am. Chem. Soc.*, 1982, **104**, 4029.

25 (*a*) V. V. Smirnov, D. W. Brinkley, M. P. Lanci, K. D. Karlin and J. P. Roth, *J. Mol. Catal. A: Chem.*, 2006, **251**, 100; (*b*) S. Epstein and T. Mayeda, *Geochim. Cosmochim. Acta*, 1953, **4**, 213.

26 T. B. Coplen, *Nature*, 1995, **375**, 285.

27 IRMS analysis was performed at Johns Hopkins University in the Department of Earth and Planetary Sciences and at the University of Waterloo Environmental Isotope Laboratory.

28 M. H. O'Leary, *Phytochemistry*, 1981, **20**, 553.

29 Non-analytic integral evaluations made use of a pruned grid having 99 radial shells and 590 angular points per shell. An automatically generated density-fitting basis set was used within the resolution-of-the-identity approximation to speed the evaluation of Coulomb integrals.

30 J. P. Perdew, Unified Theory of Exchange and Correlation Beyond the Local Density Approximation, in *Electronic Structure of Solids '91*, ed. P. Ziesche and H. Eschrig, Akademie Verlag, Berlin, 1991, pp. 11–20; C. Adamo and V. J. Barone, *Chem. Phys.*, 1998, **108**, 664–675.

31 P. J. Hay and W. R. Wadt, *J. Chem. Phys.*, 1985, **82**, 270; P. J. Hay and W. R. Wadt, *J. Chem. Phys.*, 1985, **82**, 284; P. J. Hay and W. R. Wadt, *J. Chem. Phys.*, 1985, **82**, 299.

32 (a) V. V. Smirnov, M. P. Lanci and J. P. Roth, *J. Phys. Chem. A*, 2009, **113**, 1934; (b) Calculations were carried out using the Gaussian09 package. The full citation appears in the ESI.†

33 (a) Y. Zhao and D. G. Truhlar, *J. Chem. Phys.*, 2006, **125**, 194101; (b) Y. Zhao and D. G. Truhlar, *Acc. Chem. Res.*, 2008, **41**, 157; (c) Y. Zhao and D. G. Truhlar, *Theor. Chem. Acc.*, 2008, 215.

34 D. Andrae, U. Haeussermann, M. Dolg, H. Stoll and H. Preuss, *Theor. Chim. Acta*, 1990, **77**, 123.

35 W. J. Hehre, L. Radom, P. V. R. Schleyer and J. A. Pople, *Ab Initio Molecular Orbital Theory*, Wiley, New York, 1986.

36 C. J. Cramer, *Essentials of Computational Chemistry: Theories and Models*, 2nd edn, John Wiley & Sons, Chichester, 2004.

37 A. V. Marenich, C. J. Cramer and D. G. Truhlar, *J. Phys. Chem. B*, 2009, **113**, 6378.

38 (a) T. Ziegler, A. Rauk and E. J. Baerends, *Theor. Chim. Acta*, 1977, **43**, 261; (b) L. Noodleman, *J. Chem. Phys.*, 1981, **74**, 5737; (c) C. J. Cramer and D. G. Truhlar, *Phys. Chem. Chem. Phys.*, 2009, **11**, 10757.

39 (a) K. Yamaguchi, F. Jensen, A. Dorigo and K. N. Houk, *Chem. Phys. Lett.*, 1988, **149**, 537; (b) T. Soda, Y. Kitagawa, T. Onishi, Y. Takano, Y. Shigeta, H. Nagao, Y. Yoshioka and K. Yamaguchi, *Chem. Phys. Lett.*, 2000, **319**, 223.

40 (a) L. Noodleman, C. Y. Peng, D. A. Case and J.-M. Mouesca, *Coord. Chem. Rev.*, 1995, **144**, 199; (b) I. Ciofini and C. A. Daul, *Coord. Chem. Rev.*, 2003, **238**, 187; (c) J. N. Harvey, *Struct. Bonding*, 2004, **112**, 151; (d) F. Neese, *Coord. Chem. Rev.*, 2009, **253**, 526.

41 J. Bigeleisen and M. Wolfsberg, *Adv. Chem. Phys.*, 1958, **1**, 15.

42 (a) J. P. Roth and J. P. Klinman, *Isotope Effects in Chemistry and Biology*, ed. A. Kohen and H.-H. Limbach, CRC Press, Boca Raton, FL, 2006, pp. 645–670; (b) M. Wolfsberg, *Isotope Effects in Chemistry and Biology*, ed. A. Kohen and H.-H. Limbach, CRC Press, Boca Raton, FL, 2006, pp. 1–39; (c) W. W. Cleland, *Isotope Effects in Chemistry and Biology*, ed. A. Kohen and H.-H. Limbach, CRC Press, Boca Raton, FL, 2006, pp. 915–930.

43 M. Wolfsberg, W. A. Van Hook, P. Paneth, *Isotope Effects: In the Chemical, Geological, and Bio Sciences*, Springer, New York, 2010.

44 J. Bigeleisen and M. Goeppert-Mayer, *J. Chem. Phys.*, 1947, **15**, 261.

45 W. P. Huskey, in *Enzyme Mechanism from Isotope Effects*, ed. P. F. Cook, CRC Press, Boca Raton, 1991, p. 37.

46 (a) J. A. Gilbert, D. S. Eggleston, W. R. Murphy, D. A. Geselowitz, S. W. Gersten, D. J. Hodgson and T. J. Meyer, *J. Am. Chem. Soc.*, 1985, **107**, 3855; (b) H. Yamada, W. F. Siems, T. Koike and J. K. Hurst, *J. Am. Chem. Soc.*, 2004, **126**, 9786; (c) L. Duan, F. Bozoglian, S. Mandal, B. Stewart, T. Privalov, A. Llobet and L. Sun, *Nat. Chem.*, 2012, **4**, 418; (d) D. E. Polyansky, J. T. Muckerman, J. Rochford, R. Zong, R. P. Thummel and E. Fujita, *J. Am. Chem. Soc.*, 2011, **133**, 14649; (e) M. Dooshaye, I. Alperovich, J. J. Concepcion, T. J. Meyer and Y. Pushkar, *Proc. Natl. Acad. Sci. U. S. A.*, 2013, **110**, 3765.

47 (a) M. Yoshida, S. Masaoka, J. Abe and K. Sakai, *Chem. Asian J.*, 2010, **5**, 2369; (b) A. Kimoto, K. Yamauchi, M. Yoshida, S. Masaoka and K. Sakai, *Chem. Commun.*, 2012, **48**, 239.

48 (a) A. C. Rutenburg and H. Taube, *J. Chem. Phys.*, 1952, **20**, 825; (b) H. L. Friedman, H. Taube and J. P. Hunt, *J. Chem. Phys.*, 1950, **18**, 760.

49 (a) T. Guarr, E. Buhks and G. McLendon, *J. Am. Chem. Soc.*, 1983, **105**, 3763; (b) E. Buhks, M. Bixon and J. Jortner, *J. Phys. Chem.*, 1981, **85**, 3763.

50 G. S. Huff, I. S. Doncheva, D. W. Brinkley, A. M. Angeles-Boza, A. Mukherjee, C. J. Cramer and J. P. Roth, *Biochemistry*, 2011, **50**, 7375.

51 T. F. Hughes and R. A. Friesner, *J. Phys. Chem. B*, 2011, **115**, 9280.

52 R. Bianco, P. J. Hay and J. T. Hynes, *J. Phys. Chem. A*, 2011, **115**, 8003.

53 (a) M. P. Lanci, D. W. Brinkley, K. L. Stone, V. V. Smirnov and J. P. Roth, *Angew. Chem., Int. Ed.*, 2005, **44**, 7273; (b) M. P. Lanci and J. P. Roth, *J. Am. Chem. Soc.*, 2006, **128**, 16006.

54 T. R. Weaver, T. J. Meyer, S. A. Adeyemi, G. M. Brown, R. P. Eckberg, W. E. Hatfield, E. C. Johnson, R. W. Murray and D. Untereker, *J. Am. Chem. Soc.*, 1975, **97**, 3039.

55 (a) D. Moonshiram, J. W. Jurss, J. J. Concepcion, T. Zakharova, I. Alperovich, T. J. Meyer and Y. Pushkar, *J. Am. Chem. Soc.*, 2012, **134**, 4625; (b) J. A. Stull, T. A. Stich, J. K. Hurst and R. D. Britt, *Inorg. Chem.*, 2013, **52**, 4578; (c) J. L. Cape, S. V. Lymar, T. Lightbody and J. K. Hurst, *Inorg. Chem.*, 2009, **48**, 4400.

56 X. Yang and M. H. Baik, *J. Am. Chem. Soc.*, 2006, **128**, 7476.

57 E. R. Batista and R. L. Martin, *J. Am. Chem. Soc.*, 2007, **129**, 7224.

58 (a) P. E. M. Siegbahn and R. H. Crabtree, *J. Am. Chem. Soc.*, 1999, **121**, 117; (b) G. Aullon, E. Ruiz and S. Alvarez, *Chem. – Eur. J.*, 2002, **8**, 2508; (c) P. E. M. Siegbahn and M. Lundberg, *Photochem. Photobiol. Sci.*, 2005, 1035; (d) E. M. Sproviero, J. A. Gascon, J. P. McEnvoy, G. W. Brudvig and V. S. Batista, *Philos. Trans. R. Soc., B*, 2008, **1494**, 1149; (e) M. R. A. Blomberg and P. E. M. Siegbahn, *Biochim. Biophys. Acta, Bioenerg.*, 2010, **1797**, 129; (f) I. Rivalta, G. W. Brudvig and V. S. Batista, *Curr. Opin. Chem. Biol.*, 2012, **16**, 11.

59 M. Haumann, P. Liebisch, C. Muller, M. Barra, M. Grabolle and H. Dau, *Science*, 2005, **310**, 1019.